ELSEVIER

Journal of Molecular Catalysis A: Chemical 119 (1997) 223–233

JOURNAL OF MOLECULAR CATALYSIS A: CHEMICAL

Experimental and theoretical studies of fuel cell catalysts: Density functional theory calculations of H_2 dissociation and CO chemisorption on fuel cell metal dimers

Philip C.H. Mitchell [a], Peter Wolohan [a,*], David Thompsett [b], Susan J. Cooper [b]

[a] *Department of Chemistry, University of Reading, Whiteknights, Reading RG6 2AD, UK*
[b] *Johnson–Matthey Technology centre, Sonning Common, Reading RG4 9NH, UK*

Received 6 June 1996; accepted 12 September 1996

Abstract

Gradient-corrected density functional theory (GC-DFT) calculations have been performed for molecular hydrogen, carbon monoxide and the metal dimers Pt–Pt, Pt–Ni, and Pt–Ru. The dissociative adsorption of molecular hydrogen on these metal dimers has been modelled. Derived potential energy surfaces for the dissociation of molecular hydrogen on these dimers are presented. Furthermore, the interaction with carbon monoxide has been studied. Here we find that Pt_2 binds CO significantly stronger than Pt–Ni and Pt–Ru. We present equilibrium geometries, calculated binding energies, Mulliken charge distributions, and orbital energies. Our results correlate well with our experimental studies of the hydrogen electro-oxidation reaction in a proton-exchange fuel cell where the fuel to the anode (Pt/Pt alloy on carbon electrode) is hydrogen, prepared by reforming of methane, which contains trace amounts of carbon monoxide.

Keywords: Platinum; Alloy; Density functional theory; Electrocatalyst

1. Introduction

The principle of the fuel cell [1–5] was first demonstrated by Sir William Grove in 1839, at the Royal Institution of Great Britain in London. It is an electrochemical cell in which the fuel and oxidant are continuously supplied to the cell electrodes. Although the concept was first demonstrated in the 19th century practical limitations meant that it was not until the 1950's that T. Bacon developed the first engineered prototype. The fundamental problem was, and still is, the need to obtain the highest area of contact between the electrolyte, reactants and the electrode, what Grove referred to as the, 'notable surface of action'.

The implementation of the fuel cell for transportation applications has been the driving force behind current research in the development of economically viable low-temperature fuel cells. Indeed, the solid polymer fuel cell (SPFC) [6–8] has been proposed as the ideal technology for transportation applications. The failure to transfer the engineered product to the market place has occurred mainly because of the high capital cost and insufficient power densities. A major

* Corresponding author.

PII S1381-1169(96)00486-4

contribution to the failure to deliver higher power densities from the SPFC has resulted from the deactivation of the anode electrocatalyst by trace levels of carbon monoxide (CO) in the fuel stream [9]; hence the emphasis is on the formulation of the fuel itself. Indications are that the fuel which will be most acceptable to the transportation industry is methane gas because of its natural abundance, the infrastructure for transportation is in effect already present, and the ability to obtain hydrogen via reforming, despite the fact that H_2 produced via this route contains trace amounts of CO. The need is to develop anode electrocatalysts which are effectively CO tolerant at low-temperatures. Indeed, in transportation applications the so called start-up period of the fuel cell becomes crucial. During this period the cell must provide adequate power at low-temperature while the fuel flow and hence contamination rapidly reaches its ideal operation rate so deactivating the cell.

To propel the SPFC to the forefront of the low-temperature fuel cell technologies the need is to design better CO tolerant electrocatalysts. The CO tolerance, θ_{H2}, of a carbon-supported electrocatalyst is the fraction of surface sites available to support H_2 oxidation under poisoned conditions. θ_{H2} can also be defined as the ratio of the poisoned H_2 oxidation current to pure H_2 oxidation current (surface site normalised). Here we report θ_H values for three key carbon-supported platinum-alloy electrocatalysts together with poisoned H_2 electro-oxidation specific activities.

During recent years a growing literature [10–13] has established the performance of density functional theory [14–16] (DFT) methods in predicting the properties of small molecular systems compared with experiment and correlated Hartree–Fock (HF) treatments. Increasingly gradient-corrected density functional theory [17,18] (GC-DFT) techniques have been applied to the study of gas-phase interactions with metal surfaces [19–21]. The dissociative adsorption of H_2 on various metal surfaces (Cu, Ni, Au, Pt and W) has been used as a model system [22]. At a basic level, it has been established that the energy barrier associated with H_2 dissociation which is observed for simple or noble metals arises from the orthogonalization of the metal valence d-states with the H_2 bonding molecular orbital (operation of the Pauli exclusion principle). In turn, the absence of a dissociation barrier on metals with partially filled d-states is then seen to result from the fact that orthogonalization can occur through s–d transfer of the metal electrons.

From a theoretical point of view, to develop CO tolerate anode electrocatalysts we clearly wish to model the dissociative adsorption of H_2 and the chemisorption of CO on a model which exhibits the properties of our metallic catalyst particle, including the effect of alloying platinum with, for example nickel or ruthenium. A model consisting of the guest molecule interacting with a metal dimer whose composition can be easily varied satisfies all of these criteria. Such models are not meant to represent the electrocatalyst surface but allow us to investigate the fundamental principles which dictate the marked differences observed in the H_2 and CO characteristics of these electrocatalysts.

2. Summary of computational details

The calculations presented have been performed using the DFT Gaussian-type orbital approach as implemented in the DGauss program [23]. Properties of molecules are calculated by implementing the linear combination of Gaussian-type orbitals density functional approach (LCGTAO-DFT).

All calculations presented have been performed using the Becke–Perdew [24–26] gradient correction approach (BP-DFT) implemented self-consistently in the evaluation of the wavefunction. The BP-DFT approach includes nonlocal correction terms based on the gradient of the density which correct for deviations from a uniform electron gas in the charge density. The

inclusion of such terms have been shown to improve the accuracy of calculated LDA binding energies.

A LDA optimised triple-zeta basis set with polarisation functions (TZVP) is used to describe elements H, C and O. The basis set for H is comprises of 4 contracted s-functions, constructed from 3,1,1, and 1 primitive Gaussians, and 1 contracted p-function. For C and O the basis set comprises of 4 contracted s-functions, constructed from 7, 1, 1, and 1 primitive Gaussians, 3 contracted p-functions, constructed from 4, 1 and 1 primitive Gaussians, and 1 contracted d-function.

For the metals Pt, Ni and Ru pseudopotentials have been used to relieve the burden of having to use an ab initio description of the core electrons. To generate the pseudopotential, a LDA atomic calculation is performed using the method of Troullier and Martins [27]. Relativistic effects to describe the effective charge and mass of the metal nucleus are included in the pseudopotentials. The valence basis set for use with pseudopotentials for Ni, Ru and Pt consist of 2 contracted s-functions, constructed from 4 and 3 primitive Gausians, 2 contracted p-functions, constructed from 3 and 2 primitive Gaussians, and 1 contracted d-function.

In addition to the orbital basis sets used to describe the molecular orbitals the program DGauss uses a set of auxiliary uncontracted basis functions which have shared exponents to compute the electron density, the exchange-correlation potential and exchange-correlation energy. The auxiliary basis for H is constructed from 4 primitive Gaussians to represent an s-function and 1 primitive Gaussian to represent a p-function. The auxiliary basis for C and O is constructed from 8 primitive Gaussians to represent an s-function, 4 primitive Gaussians to represent a p-function and 4 primitive Gaussians to represent a d-function. For the metals the auxiliary basis is constructed from 5 primitive Gaussians to represent an s-function, 5 primitive Gaussians to represent a p-function and 5 primitive Gaussians to represent a d-function [28].

3. Results and discussion

3.1. Observed catalytic properties

All catalysts used in this study were prepared using variations of proprietary procedures [29]. The general procedure involves the alkaline hydrolysis of the metal salts in the presence of a carbon-black slurry thus depositing the metal hydroxide on the carbon surface. The hydroxide is reduced to the metal by a number of procedures (in situ using formaldehyde or ex situ by hydrogen reduction) depending on the metal composition. The catalysts prepared are best described as finely dispersed spherical metal particles supported on high surface area graphitic carbon-blacks [30]. The metal particles have the face-centred cubic structure typical of bulk platinum and exhibit elements of different crystal faces because of defects formed at the surface of the spherical particles. Alloying in a bimetallic catalyst is induced by heating the catalyst at a high temperature in an inert atmosphere, a contraction in the lattice parameter of the alloyed catalyst particle from that of platinum being indicative of the degree of alloying.

In the electrochemical experiment a standard half cell assembly was used in the measurement of pure and poisoned hydrogen oxidation performance curves [31]. The half cell comprised of two sections; the first containing the test electrode chamber with provision for the supply of reactant gases and the second containing a platinum counter electrode and accommodated a reversible hydrogen reference electrode (RHE). For example, the procedure for measuring poisoned H_2 oxidation performance curves was as follows. The electrode was assembled, purged with nitrogen, then placed in acid electrolyte and allowed to stabilize in the chamber at the required temperature. Hydrogen gas was then passed to check the RHE whilst purging the vent line with H_2 gas containing CO. After several minutes the test electrode was exposed to the reactant gases whilst holding it at the open circuit voltage. Current voltage curves were

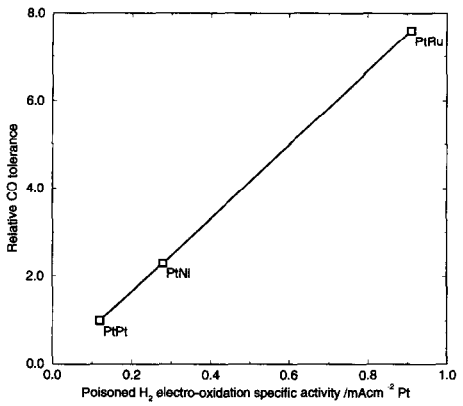

Fig. 1. Plot of observed poisoned H_2 electro-oxidation specific activity against relative CO tolerant for fuel cell electrocatalysts Pt, Pt–Ni and Pt–Ru.

recorded every 15–30 min until no further deterioration in electrode performance was observed and the internal cell resistance was measured. The corresponding specific activity is obtained by repeating these measurements at different temperatures and cell voltages while measuring the respective H_2 oxidation current. H_2 electro-oxidation has been shown to have a chemical rate determining step: dissociative chemisorption of H_2 is known as the Tafel reaction [32,33]: $H_2 + 2M = 2MH$.

The observed poisoned (100 ppm CO) H_2 electro-oxidation specific activity is plotted against the observed CO tolerance, relative to that of platinum, of three electrocatalysts; Pt, platinum–nickel (Pt–Ni) and platinum–ruthenium (Pt–Ru) in Fig. 1.

In terms of relative catalyst differences, Pt–Ru is the most CO tolerant electrocatalyst having the highest relative CO tolerance and the highest poisoned H_2 electro-oxidation specific activity, followed by Pt–Ni and Pt. Having observed this linear dependency and using our knowledge of chemical bonding we may suggest that both H_2 and CO adsorption proceed via a mechanism similar to the oxidative addition of H_2 to metal d-block complexes [34]. There are thought to be two chemical bonding steps, which proceed simultaneously but do not result in the cleavage of the H–H bond, in the oxidative addition mechanism. The first step involves a sigma type interaction between the highest occupied molecular orbital (HOMO) of the reactant and a suitable sigma orbital on the metal centre of the complex. The second step involves π-back donation via a metal d-orbital into the lowest unoccupied molecular orbital (LUMO) of the reactant. This two step picture of bonding is analogous to that used to describe the metal-ligand bonding in transition metal carbonyl complexes.

3.2. Density functional theory calculated properties

Metal dimers represent the smallest molecular system which allows us to investigate the metal–metal bond. In Table 1 we present the results of a self-consistent BP-DFT calculation of the ground state properties of the fuel cell metal dimers; Pt–Pt, Pt–Ni and Pt–Ru.

In Table 2 we present the calculated ground state properties of free H_2 and CO. As can be seen all calculated properties compare well with experiment and previously reported values from GC-DFT calculations [35,36].

In Fig. 2 we show the simple model and reaction equations used to investigate the dissociative adsorption of H_2 on the metal dimer. Our model is a T-shape configuration with the top atom always being a Pt atom. To construct a restricted potential energy surface (PES) for the corresponding process the vertical distance between the H_2 centre of gravity and metal dimer was reduced from 2.0 Å to 0.4 Å (see Fig. 3).

Table 1
Calculated ground-state properties of fuel cell metal dimers

Property	r_e	D_o	Charge distribution	
			Pt	M
Pt–Pt ($^3\Sigma_u^+$)	2.589	204	0.00	0.00
Pt–Ni ($^3\Sigma^+$)	2.385	129	−0.06	0.06
Pt-Ru ($^5\Pi$)	2.550	178	−0.03	0.03

r_e equilibrium bond length (Å), M–M D_o bond dissociation energy not zero-point energy corrected (kJ mol^{-1}) and charge distribution refers to Mulliken charge distribution ($|e^-|$).

At each vertical distance the H_2 bond length was optimised and the total energy of this optimised configuration was calculated.

Upon dissociation the H_2 splits into atomic hydrogen with each atomic hydrogen bonded to a metal atom in the dimer. After dissociation the hydrogen can split to H^+ and H^- or to $H^\cdot$ the relative energies of these two processes can be calculated by changing the multiplicity of the initial model from closed shell (H^+ and H^-) to a triplet state to ensure the occurrence of two unpaired electrons ($H^\cdot$).

The corresponding dissociation energy for the above processes on each of the fuel cell metal dimers and the calculated adsorption energy obtained at the lowest energy configuration in the PES are shown in Table 3. The corresponding restricted potential energy surface (PES) for the dissociative adsorption process on each of the fuel cell metal dimers are shown in Fig. 3.

It is striking that the calculated PES for H_2 on Pt–Pt and Pt–Ni are very similar in that they both exhibit energy minima (deep blue on the left) as H_2 approaches the dimer at a distance of 1.3 and 1.5 Å respectively. In each case at this minima the H_2 bond length is lengthen to ca. 0.9 Å, hence the molecule is not dissociated. The point at which H_2 dissociates is characterised by a H_2 bond length greater than 1.5 Å. The PES for Pt–Ru is different, the minima is now characterised by a H_2-dimer distance of 1.2 Å and a H_2 bond length of > 2.0 Å, hence the H_2 here is dissociated. However, in our model we have forced the H_2 into this configuration and in doing so it has cost energy to reach this

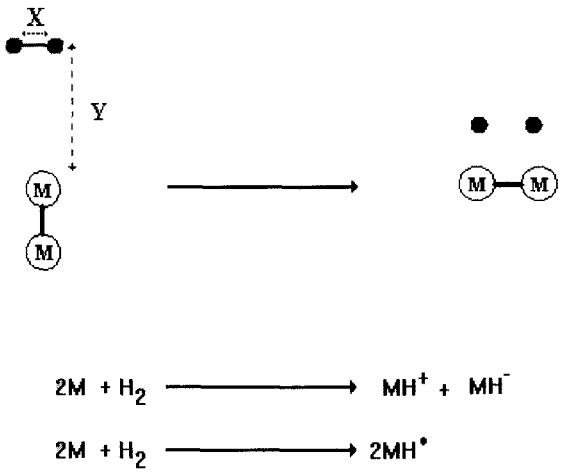

Fig. 2. Schematic of the model used to investigate the dissociation of molecular hydrogen on the fuel cell metal dimers.

point (Table 3) since the physisorption energy is very repulsive hence in reality we never reach this position. The structure in the PES at small H_2-dimer distances (< 0.8 Å) is an artifact of the calculation since we are forcing the H_2 into the dimer. However, the information obtained in doing so is of use. For example, we see that the activation energy to obtain small H_2–Pt–Pt distances is much smaller than in the alloy dimers.

To study the chemisorption of CO on the fuel cell dimers the CO molecule is allowed to optimise in a collinear configuration above the metal dimer interacting always with the Pt atom of the dimer. The total energies, equilibrium bond lengths and Mulliken charge distributions for the optimised structures are shown in Table 4.

The metal–CO bond is strongest in Pt–Pt and is characterised by a strong Pt–C bond (1.88 Å which compares well with experiment 1.85 Å,

Table 2
Calculated properties of free molecular hydrogen and carbon monoxide

Property	r_e			D_e			ω_e		
	calcd	calcd*	expt	calcd	calcd*	expt	calcd	calcd*	expt
H_2	0.750	0.748	0.741	448	432	432	4329	4373	4400
CO_2	1.145	1.150	1.128	1070	1077	1070	2111	2105	2143

r_e equilibrium bond length (Å). D_e zero-point energy corrected bond dissociation energy (kJ mol^{-1}). Charge distribution refers to Mulliken charge distribution ($|e^-|$). ω_e normal mode vibration (cm^{-1}). Experimental values taken from AIP [35]. Values in column marked calcd* refer to previously reported values using GC-DFT [36].

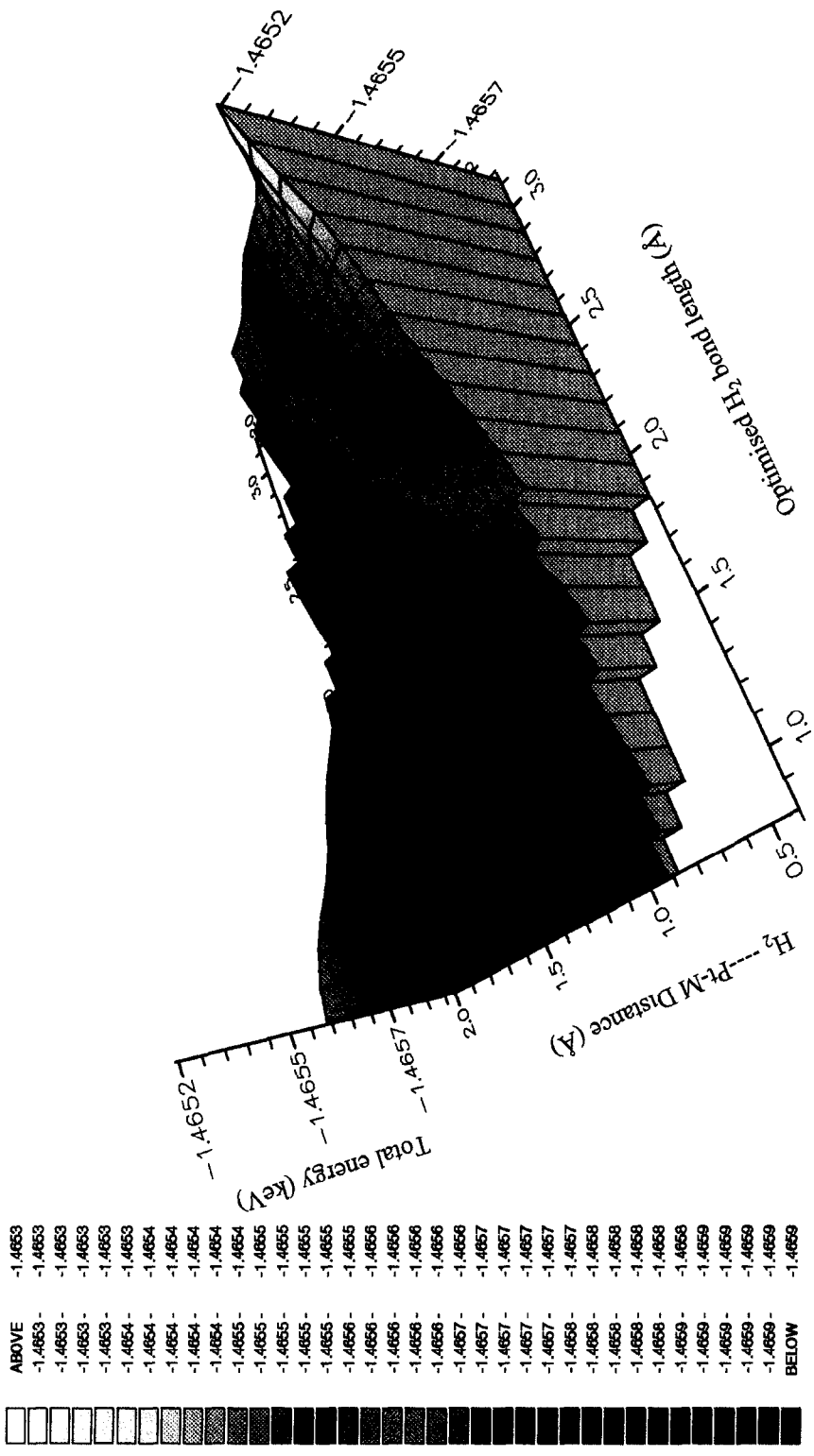

Fig. 3. Potential energy surface when H_2 interacts with each of the fuel cell metal dimers. (a) Interaction with Pt–Pt dimer. (b) Interaction with Pt–Ni dimer. (c) Interaction with Pt–Ru dimer. The energy interval between each energy grid point is 0.00002 keV, blue representing the lowest total energy and white representing the highest energy.

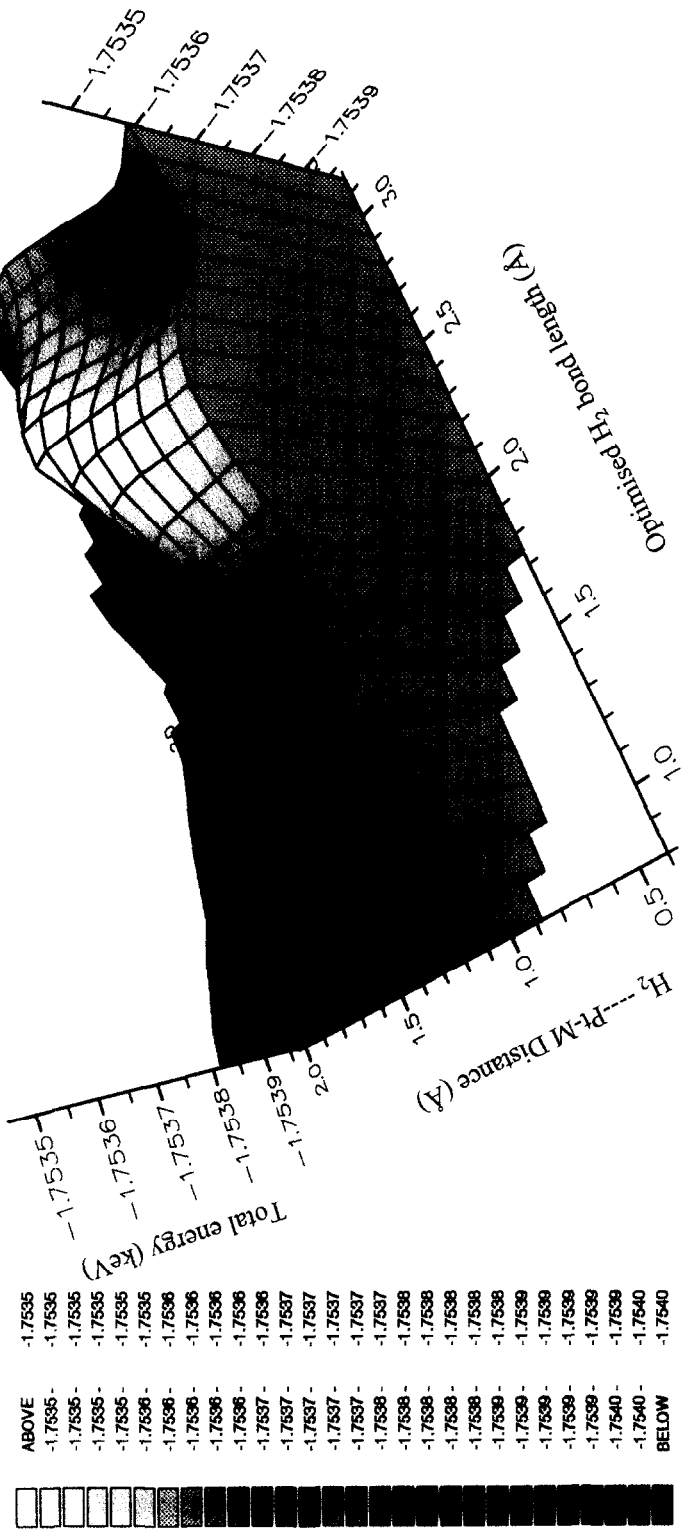

(b)

Fig. 3 (continued).

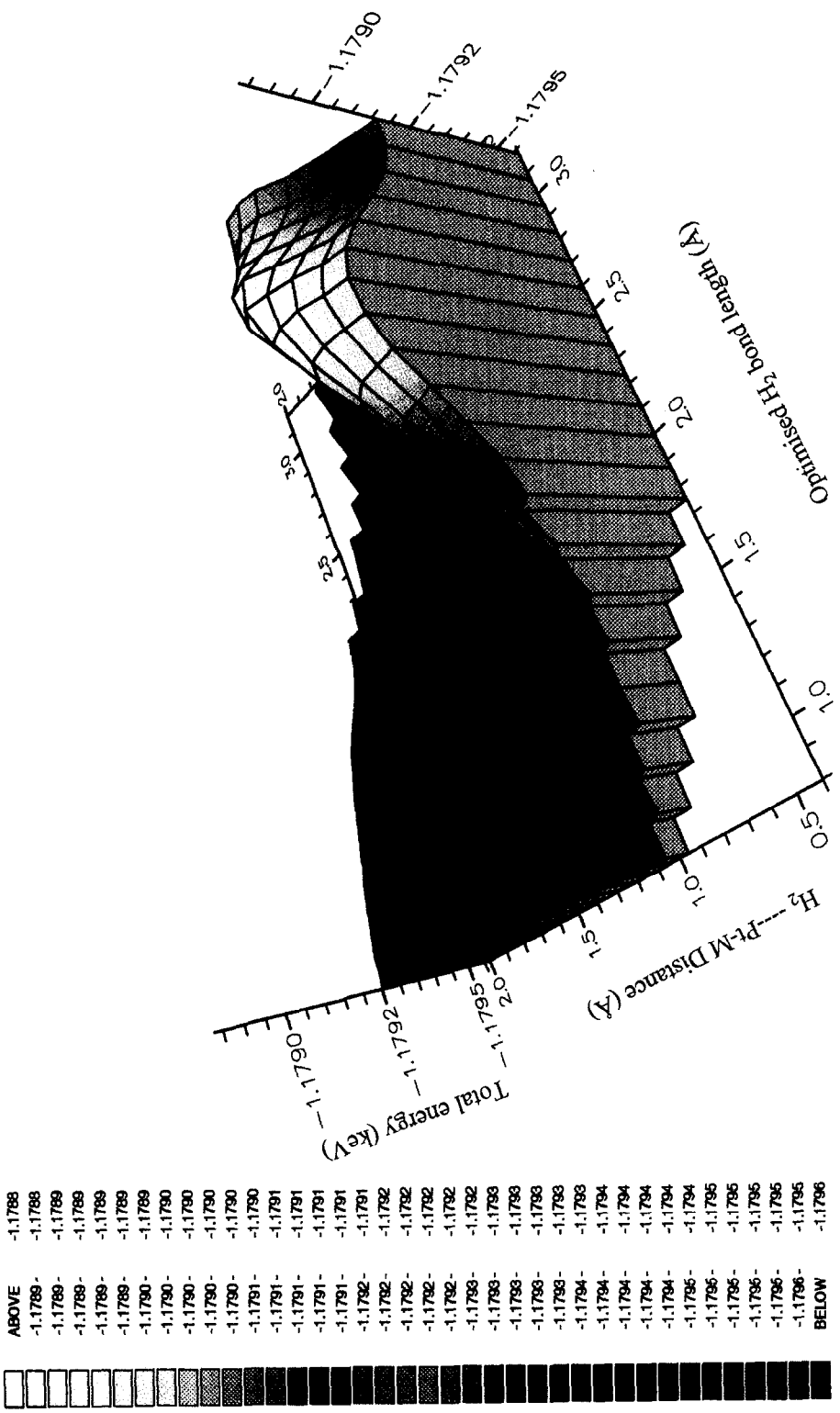

Fig. 3 (continued).

Table 3
Calculated dissociation and binding energy of molecular hydrogen on fuel cell dimers

Property	D_0 $2M + H_2 \rightarrow 2MH^{\cdot}$	D_0 $2M + H_2 \rightarrow MH^+ + MH^-$	Adsorption energy $2M + H^2 \rightarrow 2M \cdots H_2$
Pt–Pt + H_2	−98	−111	−16
Pt–Ni + H_2	−44	49	96
Pt–Ru + H_2	−58	−31	122 (139)

H_2 D_0 bond dissociation energy not zero-point energy corrected (kJ mol^{-1}). Adsorptionenergy (kJ mol^{-1}). Energy in parenthesis refers to that calculated at 1.6 Å for comparisonwith Pt–Pt and Pt–Ni energies.

CO in ontop site on bulk Pt [37]), an extension of the CO bond length by 0.017 Å and little charge transfer from CO → Pt–Pt. In Pt–Ni the Pt–C bond is weaker (1.90 Å which compares well with experiment 1.94 Å, CO in a bridge site on bulk Ni [38]), the CO bond length is effectively equivalent to that of Pt–Pt and a net transfer of charge CO → Pt–Ni is calculated (0.03|e$^-$|). The metal–CO bond is weakest in Pt–Ru and is characterised by a longer Pt–C bond length (1.925 Å) and an extension in the CO bond length by 0.019, suggesting a greater degree of π-back bonding, and a net transfer of charge Pt–Ru → CO is calculated (0.02|e$^-$|). It is obvious from these results that the formation and the relative strength of the metal–C σ bond dictates the overall strength of CO chemisorption and that the introduction of π-back bonding destabilises the metal–CO bond. This picture of metal–CO bonding is consistent with a characterisation of the orbital contributions to the first eight highest molecular orbitals of the CO adsorbed dimer system. In Pt_2 the metal–C σ bond, involving interaction between metal σ and CO $6\sigma^*$ orbital (−7.332 eV), is the most stable orbital and is more stable than the metal π^* interactions with the CO LUMO (−6.636, −6.641 eV). In Pt–Ni the metal–C σ bond (−6.677 eV) is now less stable than the metal π^* interactions with the CO LUMO and now involves a metal σ^* orbital interacting with the CO HOMO. The molecular orbitals involved in the formation of the metal–C sigma bond are dependent on the direction of charge transfer. For example, when the net charge transfer is from the metal to CO, the metal carbon bond is formed via an overlap of the metal-σ with the CO $6\sigma^*$. However, when the net charge transfer is from CO to the metal, the metal carbon bond is formed via an overlap CO 5σ with metal-σ^*. In Pt–Ru four of the first eight occupied molecular orbitals involve π-back bonding with the important metal–C σ bond (−6.365 eV) being sandwiched between two pairs of π-back bonding orbitals.

4. Conclusions

From our experimental and theoretical studies of this system we conclude the following:

• A Pt–Ru alloy electrocatalyst exhibits the best CO tolerant properties followed by a Pt–Ni

Table 4
Calculated properties of CO bound to fuel cell metal dimers

Property	r_e		Chemisorption energy	Charge distribution			
	Pt–C	C=O		M	Pt	C	O
Pt–Pt + CO	1.884	1.162	−139	0.00	−0.01	0.22	−0.21
Pt–Ni + CO	1.903	1.162	−21	0.07	−0.10	0.25	−0.22
Pt–Ru + CO	1.925	1.164	+22	0.10	−0.08	0.20	−0.22

r_e equilibrium bond length (Å). Chemisorption energy (kJ mol^{-1}). Charge distribution refers to Mulliken charge distribution (|e$^-$|).

electrocatalyst, with a Pt electrocatalyst showing the poorest CO tolerant properties.

- H_2 and CO interact in the same manner with a carbon-supported platinum or alloy electrocatalyst. Accordingly we may conclude that H_2 and Co compete for catalytic active sites in a fuel cell anode compartment.
- The traditional description of the metal–CO bond [39] being formed via a process of CO → metal* bonding and metal–CO* π-back bond donation is observed to some extent. We categorise the eight highest occupied molecular orbitals of the CO adsorbed metal–dimer system and their relative energies as being critical to the bonding process.
- The adsorption of H_2 (Table 3) and CO (Table 4) on Pt–Pt is more favourable than on Pt–Ni followed by Pt–Ru. Based on adsorption energies the Pt–CO adsorption bond is 9 times stronger than the Pt–H_2 adsorption bond.
- The effect of alloying platinum with ruthenium or nickel to form a binary alloy is to reduce the CO adsorption properties of the catalyst, the effect being purely electronic in which the second metal promotes back-donation into $2\pi^*$ LUMO. This interaction becomes more stable than the corresponding a CO-metal interaction.
- Finally by extrapolating for new alloy catalysts in Fig. 4 we hope to predict the CO tolerant characteristics of a selected alloy combination.

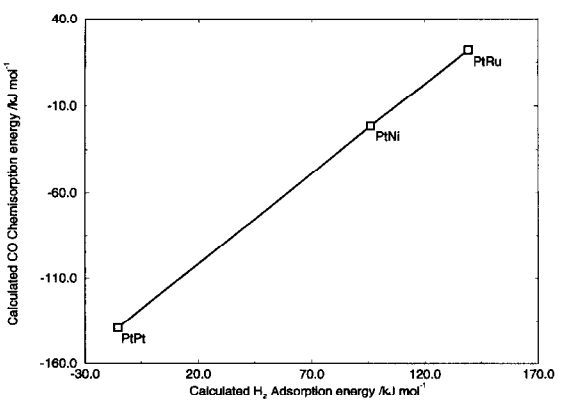

Fig. 4. Plot of calculated H_2 adsorption en energy, on fuel cell dimers.

Acknowledgements

We wish to thank the UK EPSRC and Johnson Matthey plc for providing financial support for P. Wolohan. These calculations have been performed on the Cray YMP8 at the Atlas Computing Centre using time allocated through the EPSRC supercomputing programma.

References

[1] O. Lindstrom, Chemtech 18 (1989) 409–497.
[2] M. Warshay and P.R. Prokopius, J. Power Sources 29 (1990) 193–200.
[3] K. Trimble and R. Woods, J. Power Sources 29 (1990) 37–45.
[4] N. Itoh, IEEE Spectrum 27 (1990) 40–43.
[5] S. Srinivasan, J. Electrochem. Soc. 136 (1989) 41C–48C.
[6] L.W. Niedrach and W.T. Grubb, in: W.T Mitchell, Jr. (Eds.), Fuel Cells (Academic Press, New York, 1963) p. 253.
[7] K. Prater, J. Power Sources 29 (1990) 239–250.
[8] K. Prater, J. Power Sources 37 (1992) 181–188.
[9] C.M. Seymour, J. Power Sources 37 (1992) 155.
[10] E. Wimmer, A.J. Freeman, C.-L. Fu, P.-L. Cao, S.-H. Chou and B. Delley, ACS Symp. Ser. 353 (1987)
[11] J. Labanowski and Andzelm (Eds.), Density Functional Methods in Chemistry (Springer, New York, 1991).
[12] T. Ziegler, Chem. Rev. 91 (1991) 651.
[13] R.O. Jones and O. Gunnarsson, Rev. Mod. Phys. 61 (1990) 689.
[14] P. Hohenberg and W. Kohn, Phys. Rev. B 136 (1964) 864.
[15] W. Kohn and L.J. Sham, Phys. Rev. A 140 (1965) 1133.
[16] R.G. Parr and W. Yang, Density-Functional Theory of Atoms and Molecules (Oxford University Press, New York, 1989).
[17] A.D. Becke, J. Chem. Phys. 84 (1986) 4524.
[18] C. Lee, W. Yang and R.G. Parr, Phys. Rev. B 37 (1988) 785.
[19] B. Hammer, K.W. Jacobsen and J.K. Norskov, Phys. Rev. Lett. 69 (1992) 1971.
[20] J.A. White and D.M. Bird, Chem. Phys. Lett. 213 (1993) 422.
[21] J.A. White and D.M. Bird, M.C. Payne and I. Stich, Phys. Rev. Lett. 73 (1994) 1404.
[22] K. Christmann, Surf. Sci. Rep. 9 (1989) 1.
[23] J. Andzelm and E. Wimmer, J. Chem. Phys. 96 (1992) 1280.
[24] A.D. Becke, Phys. Rev. A 38 (1988) 3098.
[25] A.D. Becke, ACS Symp. Ser. 394 (1989) 165.
[26] J.P. Perdew, Phys. Rev. B 33 (1986) 8822.
[27] N. Troullier and J.L. Martins, Phys. Rev. B 43 (1991) 1993.
[28] N. Godbout, D.R. Salahub, J. Andzelm, E. Wimmer, Can. J. Chem. 70 (1992) 560.

[29] L. Keck, J.S. Buchanan and G.A. Hards, U.S. Patent 5068161 (1991).
[30] H.J.R. Magnet, in: C. Berger (Ed.), Handbook of Fuel Cell Technology (Prentice-Hall, Englewood Cliffs, NJ, 1967).
[31] G.A. Hards, T.R. Ralph and S.J. Cooper, High Performance, Low Cost Membrane Electrode Assemblies for SPFC'S, Energy Technology Support Unit Report ETSU/FCR/002.
[32] P.N. Ross, K. Kinoshita, A.J. Scarpellino and P. Stonehart, J. Electroanal. Chem. 63 (1975) 97.
[33] P.N. Ross and P. Stonehart, J. Res. Inst. Catalysis Hokkaido Univ. 22 (1974) 22.
[34] D.F. Shriver, P.W. Atkins and C.H. Langford
[35] D.E. Gray (Ed.), American Institute of Physics Handbook (McGrawHill, New York, 1972).
[36] B.G. Johnson, P.M.W. Gill and J.A. Pople, J. Chem. Phys. 98 (1993) 5612.
[37] R.C. Baetzold, Phys. Rev. B 30 (1984) 6870.
[38] S. Andersson and J.B. Pendry, Phys. Rev. Lett. 43 (1979) 363.
[39] G. Blyholder and M.C. Allen, J. Am. Chem. Soc. 91 (1969) 3158.